Crystal structure analysis in solution-processed uniaxially oriented polycrystalline thin film of non-peripheral octahexyl phthalocyanine by grazing incidence wide-angle x-ray scattering techniques

Cite as: Appl. Phys. Lett. **109**, 153302 (2016); https://doi.org/10.1063/1.4964741
Submitted: 20 July 2016 . Accepted: 30 September 2016 . Published Online: 12 October 2016

Masashi Ohmori, Takashi Uno, Mitsuhiro Nakatani, Chika Nakano, Akihiko Fujii, and Masanori Ozaki

Crystal structure analysis in solution-processed uniaxially oriented polycrystalline thin film of non-peripheral octahexyl phthalocyanine by grazing incidence wide-angle x-ray scattering techniques

Masashi Ohmori, Takashi Uno, Mitsuhiro Nakatani, Chika Nakano, Akihiko Fujii,[a] and Masanori Ozaki
Division of Electrical, Electronic and Information Engineering, Graduate School of Engineering, Osaka University Suita, Osaka 565-0871, Japan

(Received 20 July 2016; accepted 30 September 2016; published online 12 October 2016)

Uniaxially oriented thin films of metal-free non-peripherally octahexyl-substituted phthalocyanine ($C6PcH_2$), which exhibits high carrier mobility, have been fabricated by the bar-coating technique, which is a simple solution process. The molecular orientation and molecular steps in the thin film were observed by the polarized spectroscopy and the atomic force microscopy, respectively. The three-dimensional molecular packing structure in the thin film was investigated by the grazing incidence wide-angle X-ray scattering technique with an in-plane sample rotation. The crystal orientation was clarified, and the three-dimensional molecular packing structure of the thin film was found to match the single crystal structure. Moreover, the X-ray diffraction patterns of the oriented thin films were simulated by using the lattice parameters of $C6PcH_2$ single crystal to reproduce the observed X-ray diffraction patterns. *Published by AIP Publishing.*
[http://dx.doi.org/10.1063/1.4964741]

Phthalocyanines are well known as low-molecular-weight organic semiconductors. Some of them tend to form columnar structures, which possess a π-electron stacking system along their column axis.[1] Electronic devices based on phthalocyanines, because of their stable optical and electrical properties such as solar cells and thin film transistors, have been reported.[2–4] Conventional basic phthalocyanines, that is, unsubstituted phthalocyanines, have low solubility in typical organic solvents; therefore, methods for preparing uniform thin films are limited to dry processes.[3] To realize practical applications, a solution process should be adopted because of the potential advantages of low-weight films, flexibility, low equipment cost, and large-area product.[5]

As an example of recent progress toward the application of phthalocyanines in solution-processed electronic devices, the introduction of alkyl substituents at non-peripheral positions of a phthalocyanine core has been studied.[6–10] Some non-peripherally alkyl-substituted phthalocyanines demonstrate high solubility and potential to fabricate thin films by a wet process.[9] Moreover, they exhibit high carrier mobility in the order of 10^{-1} cm^2/V s owing to their molecular packing structure based on the self-assembled columnar stacks.[11]

In particular, the non-peripherally hexyl-substituted phthalocyanine 1,4,8,11,15,18,22,25-octahexylphthalocyanine ($C6PcH_2$) exhibits a hole mobility of 1.4 cm^2/V s and an electron mobility of 0.5 cm^2/V s, which were evaluated by the time-of-flight measurement.[12] In addition, an organic thin film solar cell with a bulk hetero junction using $C6PcH_2$ exhibited a high efficiency of 4.2%.[13–15] Molecularly oriented uniform thin films are desirable for realizing high-performance electronic devices[16–18] because the origin of the electrical properties is strongly related to their molecular stacking structure, which has been studied by the X-ray diffraction (XRD) measurement[19–22] However, controlling the molecular alignment of $C6PcH_2$ in thin films still needs to be carried out.

Although spin-coating is a typical and simple method of obtaining uniform thin films, the polycrystalline or amorphous films are formed on substrates because of rapid film formation, even if materials with a strong intermolecular interaction are used. There have been several reports on the fabrication of oriented thin films by printing processes, such as inkjet and blade-coated processes.[23–25] Controlling the nucleus formation, crystal growth direction, and film formation rate is important for the crystal growth in thin film fabrication.

In this study, molecularly oriented thin films of $C6PcH_2$ were fabricated by using the bar-coating method, which is a well-known technique for the formation of uniform and large-area films.[26] The direction of film formation was uniaxially fixed by the sweep direction of the wire bar, and the conditions of film fabrication, such as the speed of film formation, the solvent, and the substrate temperature, were adjusted. In most cases of the XRD analysis, the azimuthal distribution of samples cannot be determined because the samples are fixed on a stage. In this study, the three-dimensional molecular packing structure in the obtained film was determined by applying the grazing incidence wide-angle X-ray scattering (GIWAXS) technique to the rotating sample. Moreover, the XRD patterns of the film were in excellent agreement with the results of a simulation based on the data of the single-crystal structure.[22]

Figure 1(a) shows the molecular structure of $C6PcH_2$, which was synthesized by a previously reported method.[12] The $C6PcH_2$ thin films were fabricated in the following manner. Glass substrates were cleaned with water, chloroform, acetone, and isopropyl alcohol by ultrasonication and then treated with UV-ozone. The $C6PcH_2$ thin films were fabricated on the glass

[a]E-mail: afujii@opal.eei.eng.osaka-u.ac.jp. Tel.: +81-6-6879-7758. Fax: +81-6-6879-4838.

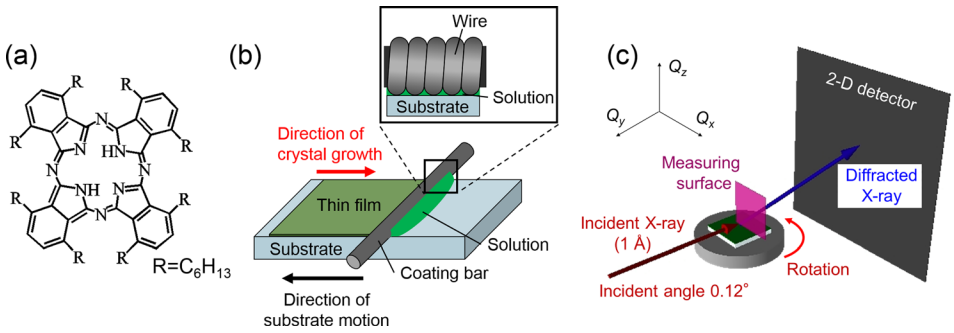

FIG. 1. (a) Molecular structure of C6PcH$_2$. (b) Schematic diagram of the bar coating process. (c) Schematic diagram of the GIWAXS measurement setup.

substrates by the bar-coating method. A schematic diagram of the bar-coating process is shown in Fig. 1(b). The substrate temperature was maintained at 40 °C. A 9.6-mm-diameter coating bar, around which a 0.05-mm-diameter metal wire was wound, was fixed on the glass substrate. C6PcH$_2$ was dissolved in *p*-xylene at a concentration of 60 mg/ml, and the solution was added dropwise onto the coating bar, and then the glass substrate was moved in the horizontal direction at a speed of 30 μm/s. A small amount of the solution passed through the space between the wound metal wire and the glass substrate, resulting in the formation of a uniform film with a thickness of approximately 170 nm.

The film thickness and surface morphology of the thin film were observed by an atomic force microscope (AFM) (KEYENCE VN-8000 or Digital Instruments Nanoscope IIIA). Polarizing optical microscopic images and polarized absorption spectra of the thin film were obtained with a polarized optical microscopic system (Nikon Eclipse LV100 POL) and an attached spectrometer (Hamamatsu PMA-11).

The GIWAXS measurement of thin film was carried out at room temperature in the BL46XU beamline at SPring-8. Figure 1(c) shows the schematic diagram of the GIWAXS measurement setup. The wavelength of the X-ray was 1.0 Å and the incident angle was 0.12°. A two-dimensional position-sensitive detector (Dectris PILATUS 300K) was used as an X-ray detector. The GIWAXS measurement was carried out, while the thin film was rotated counterclockwise at a speed of 24°/min.

The XRD patterns were simulated in the following manner. The simulation was carried out by using the crystal structure measured by the single-crystal X-ray structure analysis, which is the monoclinic structure with a space group P2$_1$/n, $a = 20.74$ Å, $b = 9.80$ Å, $c = 36.10$ Å, $\alpha = 90°$, $\beta = 93.9°$, and $\gamma = 90°$.[22] The peak positions were decided from the lattice spacing d and dihedral angle φ of the lattice planes, which were calculated by the following equations:[27]

$$\frac{1}{d^2} = \frac{1}{\sin^2\beta}\left(\frac{h^2}{a^2} + \frac{k^2\sin^2\beta}{b^2} + \frac{l^2}{c^2} - \frac{2hl\cos\beta}{ac}\right), \quad (1)$$

$$\cos\varphi = \frac{d_1 d_2}{\sin^2\beta}\left[\frac{h_1 h_2}{a^2} + \frac{k_1 k_2 \sin^2\beta}{b^2} + \frac{l_1 l_2}{c^2} - \frac{(l_1 h_2 + l_2 h_1)\cos\beta}{ac}\right], \quad (2)$$

where a, b, c, and β are lattice parameters and d_1 and d_2 are the lattice spacings of the (h_1 k_1 l_1) and (h_2 k_2 l_2) planes, respectively. The peak intensity was simulated with the RIGAKU PDXL 2.6 software.

The positions of the peaks in the azimuthal direction were simulated in the following manner. The reciprocal lattice vector $\boldsymbol{G}$ were calculated by

$$\boldsymbol{G} = h\boldsymbol{a}^* + k\boldsymbol{b}^* + l\boldsymbol{c}^*, \quad (3)$$

where h, k, and l are Miller indices and $\boldsymbol{a}^*$, $\boldsymbol{b}^*$, and $\boldsymbol{c}^*$ are basic reciprocal lattice vectors. Intersection points of the reciprocal lattice vector and Ewald sphere were calculated by

$$\varphi_{\mathrm{sam}} = \cos^{-1}\frac{\lambda|\boldsymbol{G}|^2}{4\pi\sqrt{G_x^2 + G_y^2}} - \tan^{-1}\frac{G_x}{G_y}, \quad (4)$$

where φ_{sam} is the rotating angle of the measured sample and G_x and G_y are Q_x and Q_y components of the reciprocal lattice vector, respectively. From these equations, the positions of the XRD peaks can be calculated.

Figure 2(a) shows typical polarized optical microscopic images of the thin film observed with the crossed polarizers. Some striations, which were caused by the friction of the bar-coating machine, were observed. The results show that the thin film consisted of poly-crystal. The observed image of the thin film was uniformly dark, when the polarizer was

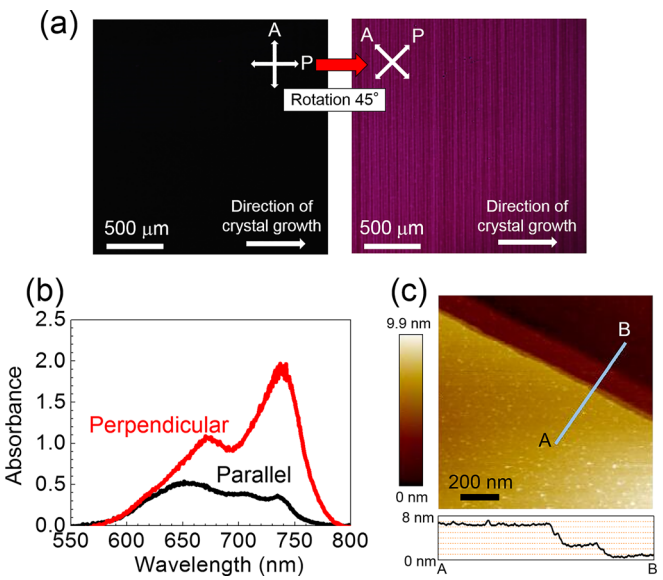

FIG. 2. (a) Polarized optical microscopic images of the thin film observed with crossed polarizers. (b) Polarized absorption spectra of the aligned thin film. The incident light was parallel (black line) or perpendicular (red line) to the crystal growth direction. (c) AFM image and surface profile of the aligned thin film. The profile corresponds to the white line in the image.

parallel to the crystal growth direction and became bright when the polarizers were rotated by 45°, which indicates that a uniform and uniaxially oriented poly-crystalline thin film with a large area was fabricated. The polarized absorption spectra of the thin film are shown in Fig. 2(b). When the polarization direction of the incident light was parallel or perpendicular to the crystal growth direction, the absorbance based on the Q-band of phthalocyanine was minimum or maximum, respectively. The absorbance should become maximum if the polarization direction of the incident light is parallel to the in-plane direction of the phthalocyanine core. Therefore, it is considered that the column axis was parallel to the crystal growth direction.

Figure 2(c) shows an AFM image and surface profile of the thin film. Terraces and steps with a height of 2 nm, which corresponded to the lattice spacing of the (002) plane in the $C6PcH_2$ single crystal,[22] were observed. This result implies that the crystal growth occurred during the film formation by the bar-coating method; moreover, the lattice vector of the (002) plane was perpendicular to the substrate.

The crystal structure in the thin film was investigated by the GIWAXS method. Figure 3(a) shows the XRD patterns, when the incident X-ray was parallel to the crystal growth direction in the bar-coating method, where $Q_{x,y}$ and Q_z are the wave numbers in the in-plane and out-of-plane directions of the thin film, respectively. Wave numbers, Q, were given by the equation $Q = 2\pi/d$, where d is the lattice spacing. Spotty XRD patterns were detected because the $C6PcH_2$ molecules were aligned on the glass substrate. Periodic XRD peaks were detected at $Q_{x,y} = 3.10\,\mathrm{nm}^{-1}$ (20.2 Å) in the in-plane direction. The periodic structures in the in-plane direction correspond to the lattice constant a (20.7 Å) of the $C6PcH_2$ single crystal, as shown in Fig. 3(b).[22] Moreover, a strong XRD peak, which corresponds to the (002) plane of the $C6PcH_2$ single crystal (18.0 Å), was detected at $Q_z = 3.52\,\mathrm{nm}^{-1}$ (17.8 Å) in the out-of-plane direction. From the coincidence between the two-dimensional lattice spacings evaluated from the XRD pattern and the lattice constants reported previously, it is considered that the molecular packing structure in the thin film was similar to that of $C6PcH_2$ single crystal and that the molecular stacking was parallel to the crystal growth direction.

Figure 3(c) shows the azimuthal dependence of the XRD pattern, obtained by integrating the XRD patterns for the in-plane direction, while the thin film was rotated by 360°. Using the GIWAXS technique involving sample rotation, it was possible to determine the azimuthal distribution in the film, which is not possible using the conventional GIWAXS technique with a fixed sample. A spotty XRD pattern was clearly obtained owing to the small azimuthal distribution based on the high orientational order in the thin film. The XRD peaks with the periods of $3.13\,\mathrm{nm}^{-1}$ (20.1 Å) and $6.26\,\mathrm{nm}^{-1}$ (10.0 Å) were detected, which almost corresponded to the lattice constants a (20.7 Å) and b (9.80 Å) of $C6PcH_2$ single crystal, respectively. Therefore, it was clarified that the fabricated thin films possessed a uniaxial orientation.

Figures 4 and 5 show the XRD patterns measured by the GIWAXS method and simulated using the data for $C6PcH_2$ single crystal, when the thin film was rotated counterclockwise by 0°, 30°, 60°, 90°, 120°, and 150°. The simulation was carried out assuming that the (002) plane was parallel to the Q_z direction. The shape of the peak in the simulation was postulated to possess a normal distribution, the standard deviation of which was assumed to be $0.01\,\mathrm{nm}^{-1}$ in the out-of-plane and in-plane directions and 2° in the azimuthal direction. The spotty XRD patterns in the longitudinal direction can be clearly observed in Figs. 4 and 5 because the Miller index l is independent of the azimuthal ($Q_{x,y}$) direction. The values of $Q_{x,y}$ at the XRD peaks and the angles of rotation of the thin film at which the peaks appeared depended on the Miller indices h and k. The values of Q_z at the XRD peaks mainly depended on the Miller index l. The Miller indices estimated by using the single crystal structure are shown in Fig. 4. From the comparison of Figs. 4 and 5, the simulated peak positions reproduced the observed ones. The comparison of the observed peak intensities and the simulated peak intensities were also carried out. The value of the R-factor calculated was 0.48, which was higher than the case of using the single crystal; however, this value was of the same level compared with the reported value of the previous study by using the highly oriented thin film.[28] The quality of the crystal in the bar-coated thin film was inferior to the single crystal; however, the highly oriented polycrystalline thin films can be fabricated.

It is considered that such uniform and uniaxially oriented thin films were obtained as a result of the properties of $C6PcH_2$, such as high solubility, high crystallinity, and uniaxial crystal growth along the molecular packing direction. The uniaxially oriented thin film is expected to be used in the electronic device applications, such as organic thin film transistors. A detailed study of the electrical properties of the thin films is now in progress, which will be reported elsewhere.

A uniform and uniaxially oriented thin film of $C6PcH_2$ was fabricated by the bar-coating method, and its three-dimensional crystal structure was investigated by the GIWAXS method with

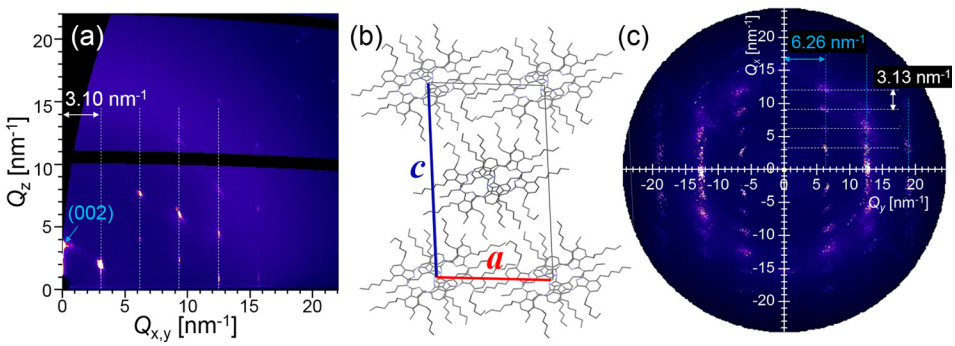

FIG. 3. (a) XRD patterns of the thin film when the incident X-ray was parallel to the crystal growth direction of the bar coating method. (b) Molecular packing structure of $C6PcH_2$ single crystal. (c) Azimuthal dependence of the XRD patterns of the thin film.

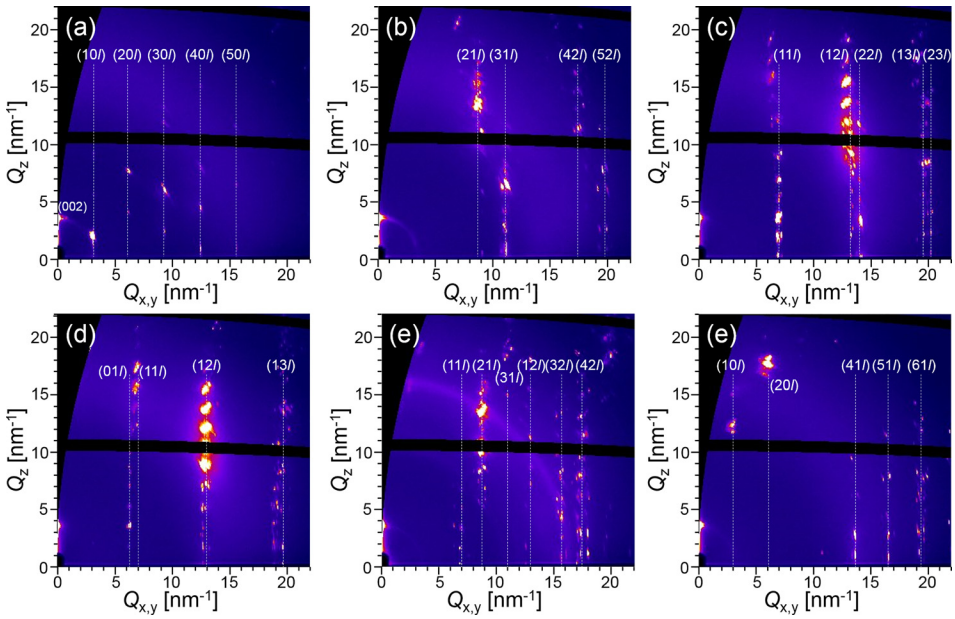

FIG. 4. XRD patterns and Miller indices of the thin film when the thin film rotated counterclockwise by 0° (a), 30° (b), 60° (c), 90° (d), 120° (e), and 150° (f). Here, the angle when the incident X-ray was parallel to the crystal growth direction of the bar coating method was set to be 0°.

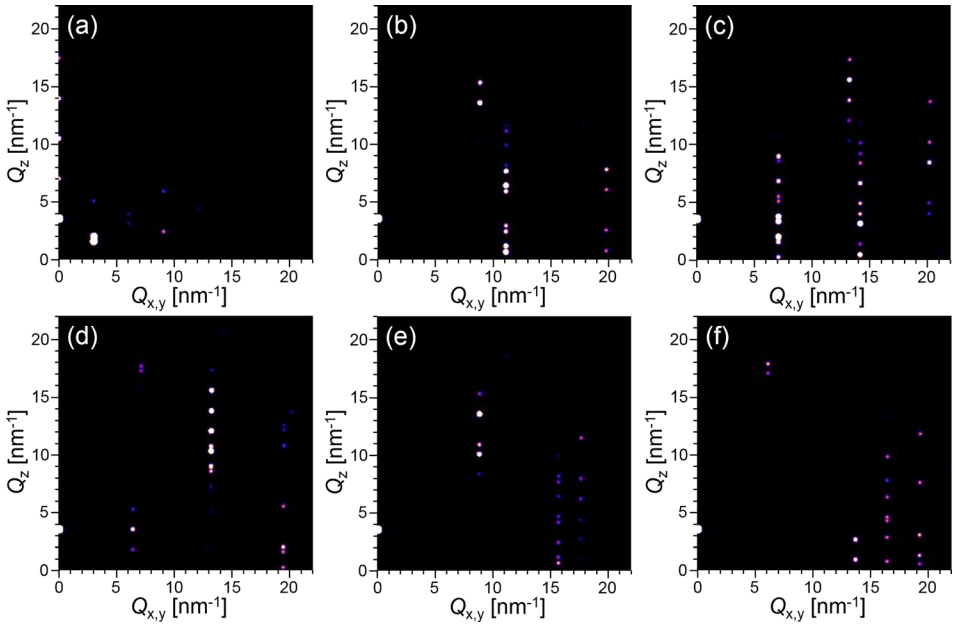

FIG. 5. Simulated patterns of the thin film by using the data of $C6PcH_2$ single crystal when the angles between the direction of the incident X-ray and the *a* axis of $C6PcH_2$ were 0° (a), 30° (b), 60° (c), 90° (d), 120° (e), and 150° (f).

a sample rotation. The fabricated thin film exhibited optically anisotropic properties over a large area and possessed molecular-size steps on the surface. From the analysis of the XRD patterns and the results of GIWAXS measurement and by comparison with the simulated results, it was clarified that the molecular packing structure in the thin film three-dimensionally coincided with that of $C6PcH_2$ single crystal and that the molecular stacking was parallel to the crystal growth direction.

The X-ray diffraction measurement in the BL46XU beamline at SPring-8 was carried out by the cooperation of the Dr. Itaru Osaka in Institute of Physical and Chemical Research (RIKEN). We thank Dr. Tomoyuki Koganezawa in the Japan Synchrotron Radiation Research Institute (JASRI) for helpful suggestions about the analysis of the XRD patterns. We appreciate Professor Koichi Sudoh of the Institute of Scientific and Industrial Research in Osaka University for helping with atomic-force microscopy. This work was partially supported by the Advanced Low Carbon Technology Research and Development Program from the Japan Science and Technology Agency and the JSPS KAKENHI Grant Nos. 15H03552, 24246009, 26600073 and a Grant-in-Aid for JSPS Fellows (No. 15J00448) from the Japan Society for the Promotion of Science and the Photonics Advanced Research Center at Osaka University.

[1]R. Zeis, T. Siegrist, and Ch. Kloc, Appl. Phys. Lett. **86**, 022103 (2005).
[2]C. W. Tang, Appl. Phys. Lett. **48**, 183 (1986).
[3]K. Sakai and M. Hiramoto, Mol. Cryst. Liq. Cryst. **491**, 284 (2008).
[4]M. Bouvet, G. Guillaud, A. Leroy, A. Maillard, S. Spirkovitch, and F. Tournilhac, Sens. Actuators, B **73**, 63 (2001).
[5]K. Yoshino, S. Nakajima, and R. Sugimoto, Jpn. J. Appl. Phys., Part 2 **26**, L1038 (1987).
[6]M. J. Cook, Chem. Rec. **2**(4), 225 (2002).
[7]H. Iino, J. Hanna, R. J. Bushby, B. Movaghar, B. J. Whitaker, and M. J. Cook, Appl. Phys. Lett. **87**, 132102 (2005).

[8]H. Iino, Y. Takayashiki, J. Hanna, and R. J. Bushby, Jpn. J. Appl. Phys., Part 1 **44**(43), L1310 (2005).
[9]T. Hori, Y. Miyake, T. Masuda, T. Hayashi, K. Fukumura, H. Yoshida, A. Fujii, Y. Shimizu, and M. Ozaki, J. Photonics Energy **2**, 021004 (2012).
[10]Q. D. Dao, T. Saito, S. Nakano, H. Fukui, T. Kamikado, A. Fujii, Y. Shimizu, and M. Ozaki, Appl. Phys. Express **6**, 122301 (2013).
[11]A. S. Cherodian, A. N. Davies, R. M. Richardson, M. J. Cook, N. B. Mckeown, A. J. Thomson, J. Feijoo, G. Ungar, and K. J. Harrison, Mol. Cryst. Liq. Cryst. **196**, 103 (1991).
[12]Y. Miyake, Y. Shiraiwa, K. Okada, H. Monobe, T. Hori, N. Yamasaki, H. Yoshida, M. J. Cook, A. Fujii, M. Ozaki, and Y. Shimizu, Appl. Phys. Express **4**, 021604 (2011).
[13]T. Hori, Y. Miyake, N. Yamasaki, H. Yoshida, A. Fujii, Y. Shimizu, and M. Ozaki, Appl. Phys. Express **3**, 101602 (2010).
[14]M. Ohmori, H. Fukui, Q. D. Dao, T. Kumada, A. Fujii, Y. Shimizu, and M. Ozaki, Jpn. J. Appl. Phys., Part 1 **53**, 05FZ02 (2014).
[15]Q. D. Dao, T. Hori, K. Fukumura, T. Masuda, T. Kamikado, A. Fujii, Y. Shimizu, and M. Ozaki, Org. Electron. **14**, 2628 (2013).
[16]V. D. Cupere, J. Tant, P. Viville, R. Lazzaroni, W. Osikowicz, W. R. Salaneck, and Y. H. Greerts, Langmuir **22**, 7798 (2006).
[17]E. Pouzet, V. D. Cupere, C. Heintz, J. W. Andreasen, D. W. Breiby, M. M. Nielsen, P. Vivile, R. Lazzaroni, G. Gbabode, and Y. H. Greerts, J. Phys. Chem. C **113**, 14398 (2009).
[18]B. P. Rand, D. Cheyns, K. Vasseur, N. C. Giebink, S. Mothy, Y. Yi, V. Coropceanu, D. Beljonne, J. Cornil, J. Bredas, and J. Genoe, Adv. Funct. Mater. **22**, 2987 (2012).
[19]I. Chambrier, M. J. Cook, M. Helliwell, and A. K. Powell, J. Chem. Soc., Chem. Commun. **1992**, 444.
[20]M. Yoneya, A. Miyamoto, Y. Shimizu, A. Fujii, and M. Ozaki, J. Phys. Chem. C **119**(42), 23852 (2015).
[21]M. Ohmori, T. Higashi, A. Fujii, and M. Ozaki, J. Nanosci. Nanotechnol. **16**, 3318 (2016).
[22]M. Ohmori, C. Nakano, T. Miyano, N. Tohnai, A. Fujii, and M. Ozaki, J. Cryst. Growth **445**, 9 (2016).
[23]K. Nakayama, Y. Hirose, J. Soeda, M. Yoshizumi, T. Uemura, M. Uno, W. Li, M. J. Kang, M. Yamagishi, Y. Okada, E. Miyazaki, Y. Nakazawa, A. Nakao, K. Takimiya, and J. Takeya, Adv. Mater. **23**, 1626 (2011).
[24]H. Minemawari, T. Yamada, H. Matsui, J. Tsutsumi, S. Haas, R. Chiba, R. Kumai, and T. Hasegawa, Nature **475**, 364 (2011).
[25]J. Soeda, T. Uemura, T. Okamoto, C. Mitsui, M. Yamagishi, and J. Takeya, Appl. Phys. Express **6**, 076503 (2013).
[26]D. Khim, H. Han, K. Baeg, J. Kim, S. Kwak, D. Kim, and Y. Noh, Adv. Mater. **25**, 4302–4308 (2013).
[27]B. D. Cullity, *Elements of X-Ray Diffraction*, 2nd ed. (Addison-Wesley, Sydney, 1978), pp. 501–503.
[28]T. Watanabe, T. Koganezawa, M. Kikuchi, C. V. Ackermann, J. Ackermann, H. Brisset, I. Hirosawa, and N. Yoshimoto, Jpn. J. Appl. Phys., Part 1 **53**, 01AD01 (2014).